Functional integration of "undead" neurons in the olfactory system

Lucia L. Prieto-Godino[1,#,+], Ana F. Silbering[1,#], Mohammed A. Khallaf[2,¥], Steeve Cruchet[1,¥], Karolina Bojkowska[3], Sylvain Pradervand[3,4], Bill S. Hansson[2], Markus Knaden[2] and Richard Benton[1,*]

[1]Center for Integrative Genomics
Faculty of Biology and Medicine
University of Lausanne
CH-1015 Lausanne
Switzerland

[2]Department of Evolutionary Neuroethology
Max Planck Institute for Chemical Ecology
D-07745 Jena
Germany

[3]Genomic Technologies Facility
Faculty of Biology and Medicine
University of Lausanne
CH-1015 Lausanne
Switzerland

[4]Vital-IT Group, SIB
Swiss Institute of Bioinformatics
CH-1015 Lausanne
Switzerland

[+]Present address: The Francis Crick Institute, 1 Brill Place, London, NW1 1BF, United Kingdom

[#]These authors contributed equally to this work
[¥]These authors contributed equally to this work

[*]Corresponding author:
T: ++41 21 692 3932
E: Richard.Benton@unil.ch

Abstract:

Programmed cell death (PCD) is widespread during neurodevelopment, typically countering the surpluses of neuronal production. We examined, in the *Drosophila* olfactory system, the potential of cells fated to die to contribute to circuit evolution. Inhibition of PCD is sufficient to generate many new cells that express neural markers and exhibit odor-evoked activity. These “undead” neurons express a subset of olfactory receptors, enriched for recent receptor duplicates, and including those normally found in other chemosensory organs and life-stages. Moreover, undead neuron axons integrate into the olfactory circuitry in the brain. Comparison of homologous olfactory lineages across drosophilids reveals natural examples of fate changes from death to a functional neuron. These results reveal the remarkable potential of alterations in patterns of PCD to evolve novel neural pathways.

Main text:

A fundamental way in which nervous systems evolve is through increases in the numbers of neurons (*1-3*). Additional sensory neurons can enable higher sensitivity to environmental signals or lead to functional diversification to support acquisition of novel detection abilities. Increases in central neuron number might underlie diverse enhancements in cognitive abilities (*4*), such as parallel processing and memory storage. The generation of more neurons could be achieved through greater production during development – by increasing the number and/or proliferation of neural precursor cells – a process that appears to underlie neocortical expansion

during primate evolution (*5*). Alternatively (or additionally), given the widespread occurrence of programmed cell death (PCD) during neural development (*6, 7*), prevention of this process can potentially yield a pool of additional neurons. Consistent with this idea, genetic blockage of PCD in mice or *D. melanogaster* results in the development of enlarged, albeit malformed, nervous systems (*8, 9*). Moreover, in *C. elegans*, the function of an experimentally-ablated pharyngeal neuron can be partially compensated by a sister cell rescued from PCD by a caspase mutation (*10*).

Here we examined the potential of PCD blockage in the formation of novel neural pathways in the *D. melanogaster* olfactory system. This model is of interest because its development involves prevalent PCD and its molecular neuroanatomy is well-described. The principal olfactory organ, the third antennal segment, is covered with ~400 porous sensory hairs (sensilla) of morphologically-diverse classes (Fig. 1A) (*11*). An individual sensillum derives from a single sensory organ precursor (SOP) cell that is specified in the antennal imaginal disc (*12, 13*). Each SOP gives rise to a short, fixed lineage of asymmetric cell divisions that produces eight terminal cells with distinct identities (*13, 14*) (Fig. 1B). Four adopt non-neural ("support cell") fates, and are involved in the construction of the hair, amongst other roles. The other four cells can potentially differentiate as olfactory sensory neurons (OSNs), which express a single (or rarely two) sensory receptor genes, develop ciliated dendrites that innervate the lumen of the sensillum hair, and project axons towards a specific glomerulus in the primary olfactory centre in the brain (antennal lobe). There are ~20 sensillum classes, housing stereotyped combinations of OSNs (Data S1) (*15-17*). Of

these, only one class (antennal basiconic 1 [ab1]) contains four neurons, with the others containing fewer – mostly two or three – OSNs. The "missing" neurons are removed by PCD ~22-32 hours after puparium formation (APF) (*14, 18-20*), when OSN terminal fate is established (*21*).

To block PCD during OSN development, we first used animals bearing deletions in the tandem cluster of pro-apoptotic genes (*head involution defective* (*hid*), *grim*, *reaper* (*rpr*) and *sickle* (*skl*)), which encode transcription factors critical for promoting developmentally-regulated PCD in diverse tissues (Fig. 1C) (*22, 23*). Homozygous chromosomal deficiencies that span the entire cluster cause embryonic lethality. However, a trans-heterozygous combination (*Df(3L)H99/Df(3L)XR38*), which removes both copies of *rpr*, and one copy each of *hid*, *grim* and *skl*, allowed recovery of a few viable adults. Immunofluorescence on whole-mount antennae with an antibody against the neural nuclear marker, Elav, revealed a clear increase in the number of labelled cells in mutant animals compared to controls (Fig. 1D), indicating that new neurons form when cell death is prevented.

PCD might be impaired in these mutants at any stage of olfactory system development, including during SOP specification. To selectively block the terminal PCD of OSN lineages (Fig. 1B), we down-regulated expression of *hid*, *grim* and *rpr* by transgenic RNAi from ~18 h APF using the *pebbled-Gal4* (*peb-Gal4*) driver, which is broadly-expressed in post-mitotic terminal OSN precursors (*24*). Blockage of OSN-specific PCD in this manner also led to a significant increase in Elav-positive cells (Fig. 1E). The number of extra Elav-positive cells observed in these experiments (~200-300, recognising the limits of automated neuron counting in nuclei-dense

tissue (Fig. S1)) is in line with estimates of the total number of potential undead neurons (~300-400) (Data S1). We further confirmed the role of the PCD pathway in the antenna through expression of the baculoviral caspase inhibitor p35 (*25*) with the same driver. *peb-Gal4>UAS-p35* (hereafter "PCD-blocked") animals displayed higher numbers of Elav-positive cells compared to a *peb-Gal4* (control) (Fig. 1F), consistent with a caspase-dependent PCD pathway in this sensory organ.

To determine whether these additional Elav-positive cells are functional neurons, we performed single-sensillum electrophysiological recordings. We focused on one class of trichoid sensilla, at1, which houses a single OSN in wildtype animals, due to PCD of the other three potential neurons in the lineage (*20*). This OSN expresses OR67d, a receptor for the pheromone *11-cis*-vaccenyl acetate (cVA) (*26*). at1 sensilla are easily recognized by their sparse basal (spontaneous) pattern of spikes of a single amplitude, and the robust train of spikes that occur only upon cVA presentation (Fig. 2A,D). In PCD-blocked animals, these sensilla often contain additional spikes of smaller amplitude (Fig. 2B-C), suggesting the presence of one or more extra, active OSNs (spike amplitude is defined by the OSN not the receptor gene (*27*)). Moreover, exposure to a blend of food-derived odors (which activate many different ORs (*28*)) led to responses of the undead neurons in about one-third of the tested sensilla (Fig. 2D-E); the non-responding undead neurons may express receptors activated by other stimuli. These observations indicate that blocking PCD can lead to the development of functional OSNs. The variable odor-evoked responses of these undead neurons to food-derived odors (Fig. 2E) suggests that

these cells do not have a fixed identity in at1 sensilla but rather express one of several different types of receptors.

To identify the receptor genes expressed by undead OSNs, we performed comparative transcriptomics of whole antennae of control and PCD-blocked animals by RNA-sequencing. As a positive control, we first examined the changes in transcript levels of *grim*, *rpr*, *hid* and *skl*, reasoning that inhibition of PCD downstream in the pathway should lead to the presence of undead cells expressing mRNAs for these pro-apoptotic genes (Fig. 1C). Indeed, three of these genes showed higher expression levels in PCD-blocked antennae (Fig. 3A).

We next queried the transcript levels for all chemosensory receptors, comprising *Odorant receptor* (*Or*), *Ionotropic receptor* (*Ir*) and *Gustatory receptor* (*Gr*) gene families (Extended Data Tables 1-2). Of the receptors previously detected in antennal neurons *in situ* (*15, 16, 29*), we found that 10/36 *Or*s, 1/17 *Ir*s and 0/3 *Gr*s displayed a >1.5-fold increase in expression, suggesting that only subsets of these receptors are expressed in the undead neurons (Fig. 3A-B and Extended Data Tables 2-3).

To validate these transcriptomic data, we visualized the neuronal expression of several of the *Or*s *in situ*. Transcripts for all of those tested by RNA fluorescent *in situ* hybridisation (FISH) were detected in more neurons in PCD-blocked antennae compared to controls (Fig. 3C and Fig. S2A). In some cases, these neurons were found only within the same region of the antenna as the endogenous OSNs (e.g., *Or42b*, *Or65a*) while in others (e.g., *Or19a*, *Or43a*) undead neurons were observed in novel locations (Fig. 3C and Fig. S2B).

Notably, many of the other receptors displaying increases in transcript levels normally act in other chemosensory organs, including one *Or* expressed in the maxillary palp (*Or85e*), two larval *Or*s, and seven *Gr* genes, which function in various gustatory organs (Fig. 2A and Extended Data Tables 2-3). *In situ* analysis revealed the presence of transcripts for *Or85e* and the larval-specific *Or33b* in populations of undead neurons in PCD-blocked antennae (Fig. 3D).

Beyond these cases, the RNA levels of the vast majority of receptor genes were either unchanged or slightly down-regulated in PCD-blocked antennae (Fig. 3A and Data S2). Consistently, *in situ* analysis of a sample of antennal genes revealed only a very small increase (e.g., Ir75c), no change (e.g., Or13a, Or67d, Ir75b), or a decrease (e.g., Or35a, Or22a) in the size of the corresponding neuron populations (Fig. 3E, and Fig. S2C). The latter, unexpected phenotype raises the possibility that undead neurons impact (directly or indirectly) the specification and/or survival of certain populations of neurons.

What properties characterize the small subset of receptors that are expressed in undead neurons? They are normally expressed in neurons housed in diverse sensillum types: basiconic (e.g., *Or42b*), trichoid (e.g., *Or65a*), intermediate (e.g., *Or19a*), and coeloconic (e.g., *Ir75d*) (Fig. 3B). By contrast, most of these receptors (including 9/10 *Or*s) are activated in OSNs derived from the Nba precursor cell; the remaining *Or* (*Or43a*) and the sole *Ir* (*Ir75d*) are expressed in Naa-derived OSNs (Fig. 1B and Data S3). This pattern suggests that undead neurons (which are largely Naa-derived (Fig. 1B) preserve gene-regulatory networks that are more similar to Nba/Naa cells than Nab cells, perhaps reflecting the shared Notch activity in Naa

and Nba precursors (Fig. 1B) (*13*). Finally, of the 13 *Or*s detected in undead neurons (including those from other olfactory organs), ten are normally co-expressed with other *Or* genes, a striking enrichment given the rarity of receptor co-expression within this repertoire (*15, 29*). While some co-expressed receptors remain co-expressed in undead OSNs (*e.g., Or65a* and *Or65b* (Fig. S2D)), this is not always the case. For example, *Or19a*, but not the co-expressed *Or19b*, displays up-regulation by RNA-seq (Data S2). In addition, *in situ* analysis of *Or49a* (using an *Or49a*-CD8:GFP (*Or49a*-GFP) reporter (*15*)) and *Or85f*, reveals that while these are always co-expressed in control antennal OSNs, in PCD-blocked antennae there is a novel population of undead neurons that expresses *Or49a*-GFP, but not *Or85f* (Fig. 3F).

We next investigated whether undead OSNs project their axons to the antennal lobe. To label these neurons, we used an EGFP gene trap allele of *grim* (*grim*$^{MI03811(EGFP)}$), in which the fluorophore should report on the expression pattern of this pro-apoptotic gene. In controls, *grim*$^{MI03811(EGFP)}$ expression is detected only at background levels across the antenna; this is expected, as cells that induce *grim* (and so EGFP) expression are fated to die (Fig. 4A). By contrast, in PCD-blocked antennae, EGFP was detected in many soma (Fig. 4A), which presumably represent the undead neurons previously observed with Elav antibodies (Fig. 1F). In the brains of these animals, we observed that the EGFP-labelled neurons innervate multiple glomeruli of the antennal lobe, indicating that undead neurons can form axonal projections to the primary olfactory centre. Antennal deafferentation experiments

confirmed that the specific glomerular signals in PCD-blocked animals were entirely due to the contribution of OSNs (Fig. 4B).

Although the global architecture of the antennal lobe, as visualized by the synaptic marker nc82 (Bruchpilot), is similar in control and PCD-blocked animals, we did detect minor, and somewhat variable, morphological differences, including less distinct boundaries between certain glomeruli and apparently novel regions of neuropil. We wondered whether these differences reflect the innervation patterns of populations of undead OSNs. To test this possibility, we examined the projections of the neurons expressing the *Or49a*-GFP reporter, which labels many more neurons in PCD-blocked antennae; some of these are different from control neurons as they do not co-express *Or85f* (Fig. 3F). In control animals, these neurons project to a single glomerulus, DL4, as previously described (*15*). In PCD-blocked animals, labelled axons projected to DL4, as well as to a second, more anterior, glomerulus-like structure (Fig. 4C), which presumably correspond to the wild-type Or49a neuron population and the undead neurons that express this reporter, respectively (Fig. 3F). This observation suggests that undead neurons can acquire distinct fates from control neurons, both by expressing distinct receptor combinations and by forming different glomerular targets in the brain.

We next asked whether such novel OSN axons can potentially synapse with second-order projection neurons (PN). We combined the *Or49a*-GFP reporter with a genetic driver for the majority of PNs (*GH146-QF>QUAS-Tomato*) in control and antennal PCD-blocked flies. GH146-labelled processes were detected in the novel *Or49a*-GFP-labelled glomerulus (Fig. 4F). Moreover, nc82 immunoreactivity, which

reflects the presence of the active zone scaffolding protein Bruchpilot (*30*) was also detected in this region (Fig. 4C), implying the formation of synapses between OSNs and these second order neurons. The novel connectivity does not result from the production of additional PNs (Fig. 4E), suggesting that there is no mechanism to match OSN and PN numbers.

Our demonstration that inhibition of PCD is sufficient to allow the development of new functional OSN populations that integrate into the olfactory circuitry is consistent with the hypothesis that modulation of cell death patterns during evolution can be a mechanism to create (or, conversely, remove) olfactory channels. While the variation in OSN number per sensilla within *D. melanogaster* implies that different SOP lineages have distinct regulation of PCD, we wondered whether we could identify examples of divergent PCD patterning across shorter evolutionary timescales by comparing homologous sensilla in different drosophilids. Previous cross-species analyses suggested this is likely to be relatively rare, as no differences in neuron numbers or pairing were reported in at least a subset of basiconic and coeloconic sensilla in a limited range of drosophilids (although receptor tuning properties do vary) (e.g., (*31-33*)). We therefore performed a broader electrophysiological screening of at1 sensilla in 24 drosophilid species. While the at1 sensilla of most species house a single cVA-responsive neuron (Fig. 5A), similar to *D. melanogaster*, we identified several species in which this sensillum houses two neurons of distinct spike amplitudes (Fig. 5B), only one of which is cVA-responsive. The lack of genomic of these species currently precludes further molecular analysis, although we assume that cVA-responsive neurons express an OR67d ortholog and

the partner neurons a distinct OR of still-unknown sensory specificity. The at1 phenotype in these species is reminiscent of that observed in *D. melanogaster* when PCD was inhibited (Fig. 2) and provides natural examples of potential changes in PCD patterns leading to novel neuronal circuit elements. Mapping the species whose at1 sensilla house >1 OSN onto a phylogenetic tree, reveals that the acquisition of an additional neuron has occurred independently multiple times during the diversification of the drosophilid clade (Fig. 5C).

A future challenge will be to understand how PCD is determined in OSN lineages and how these mechanisms relate to those defining the fate of the OSNs that survive and express specific receptor genes. Our RNA-seq dataset provides a molecular entry-point to answer these questions by identifying candidate genes expressed highly in cells normally fated to die, similar to the pro-apoptotic factors. Such knowledge is an essential pre-requisite to address how PCD pathways are modified during evolution to selectively eliminate or create OSN populations.

One intriguing observation is that undead neuron populations do not necessarily exhibit functional or anatomical properties that match those of existing OSNs, for example, by expressing receptor genes not normally activated in antennal neurons, or just one of two normally co-expressed receptors. These traits presumably reflect properties of undead OSNs' "latent" gene regulatory networks. Our work, together with a related study (*34*), reveals the outstanding potential for modulation of cell death patterns to generate new neurons with unique functions and wiring patterns.

References and Notes

1. Z. Han, S. Boas, N. E. Schroeder, Unexpected Variation in Neuroanatomy among Diverse Nematode Species. *Frontiers in neuroanatomy* **9**, 162 (2015).
2. S. Herculano-Houzel, K. Catania, P. R. Manger, J. H. Kaas, Mammalian Brains Are Made of These: A Dataset of the Numbers and Densities of Neuronal and Nonneuronal Cells in the Brain of Glires, Primates, Scandentia, Eulipotyphlans, Afrotherians and Artiodactyls, and Their Relationship with Body Mass. *Brain Behav Evol* **86**, 145 (2015).
3. N. J. Strausfeld, I. Sinakevitch, S. M. Brown, S. M. Farris, Ground plan of the insect mushroom body: functional and evolutionary implications. *J Comp Neurol* **513**, 265 (Mar 20, 2009).
4. W. Q. Fang, R. Yuste, Overproduction of Neurons Is Correlated with Enhanced Cortical Ensembles and Increased Perceptual Discrimination. *Cell Rep* **21**, 381 (Oct 10, 2017).
5. M. Wilsch-Brauninger, M. Florio, W. B. Huttner, Neocortex expansion in development and evolution - from cell biology to single genes. *Curr. Opin. Neurobiol.* **39**, 122 (Aug, 2016).
6. M. P. Dekkers, V. Nikoletopoulou, Y. A. Barde, Cell biology in neuroscience: Death of developing neurons: new insights and implications for connectivity. *J Cell Biol* **203**, 385 (Nov 11, 2013).
7. Y. Yamaguchi, M. Miura, Programmed cell death in neurodevelopment. *Dev Cell* **32**, 478 (Feb 23, 2015).

8. K. Kuida *et al.*, Reduced apoptosis and cytochrome c-mediated caspase activation in mice lacking caspase 9. *Cell* **94**, 325 (Aug 7, 1998).

9. A. Rogulja-Ortmann, K. Luer, J. Seibert, C. Rickert, G. M. Technau, Programmed cell death in the embryonic central nervous system of *Drosophila melanogaster*. *Development* **134**, 105 (Jan, 2007).

10. L. Avery, H. R. Horvitz, A cell that dies during wild-type *C. elegans* development can function as a neuron in a ced-3 mutant. *Cell* **51**, 1071 (Dec 24, 1987).

11. S. R. Shanbhag, B. Muller, R. A. Steinbrecht, Atlas of olfactory organs of *Drosophila melanogaster*. 1. Types, external organization, innervation and distribution of olfactory sensilla. *Int J Insect Morphol Embryol* **28**, 377 (Oct 1, 1999).

12. V. Rodrigues, T. Hummel, Development of the *Drosophila* olfactory system. *Adv Exp Med Biol* **628**, 82 (2008).

13. K. Endo *et al.*, Chromatin modification of Notch targets in olfactory receptor neuron diversification. *Nature Neuroscience* **15**, 224 (2011).

14. K. Endo, T. Aoki, Y. Yoda, K. Kimura, C. Hama, Notch signal organizes the *Drosophila* olfactory circuitry by diversifying the sensory neuronal lineages. *Nat. Neurosci.* **10**, 153 (Feb, 2007).

15. A. Couto, M. Alenius, B. J. Dickson, Molecular, anatomical, and functional organization of the *Drosophila* olfactory system. *Curr Biol* **15**, 1535 (Sep 6, 2005).

16. R. Benton, K. S. Vannice, C. Gomez-Diaz, L. B. Vosshall, Variant ionotropic glutamate receptors as chemosensory receptors in *Drosophila*. *Cell* **136**, 149 (Jan 9, 2009).

17. V. Grabe *et al.*, Elucidating the Neuronal Architecture of Olfactory Glomeruli in the *Drosophila* Antennal Lobe. *Cell Rep* **16**, 3401 (Sep 20, 2016).

18. G. V. Reddy, B. Gupta, K. Ray, V. Rodrigues, Development of the *Drosophila* olfactory sense organs utilizes cell-cell interactions as well as lineage. *Development* **124**, 703 (Feb, 1997).

19. A. Sen, D. Kuruvilla, L. Pinto, A. Sarin, V. Rodrigues, Programmed cell death and context dependent activation of the EGF pathway regulate gliogenesis in the *Drosophila* olfactory system. *Mech Dev* **121**, 65 (Jan, 2004).

20. P. C. Chai, S. Cruchet, L. Wigger, R. Benton, Sensory neuron lineage mapping and manipulation in the *Drosophila* olfactory system. *Nat Commun* **10**, 643 (Feb 7, 2019).

21. G. S. Jefferis, T. Hummel, Wiring specificity in the olfactory system. *Semin Cell Dev Biol* **17**, 50 (Feb, 2006).

22. G. Lee *et al.*, Essential role of grim-led programmed cell death for the establishment of corazonin-producing peptidergic nervous system during embryogenesis and metamorphosis in *Drosophila melanogaster*. *Biology open* **2**, 283 (Mar 15, 2013).

23. F. Pinto-Teixeira, N. Konstantinides, C. Desplan, Programmed cell death acts at different stages of *Drosophila* neurodevelopment to shape the central nervous system. *FEBS Lett* **590**, 2435 (Aug, 2016).

24. L. B. Sweeney *et al.*, Temporal target restriction of olfactory receptor neurons by Semaphorin-1a/PlexinA-mediated axon-axon interactions. *Neuron* **53**, 185 (Jan 18, 2007).

25. B. A. Hay, T. Wolff, G. M. Rubin, Expression of baculovirus P35 prevents cell death in *Drosophila*. *Development* **120**, 2121 (Aug, 1994).

26. T. S. Ha, D. P. Smith, A pheromone receptor mediates 11-*cis*-vaccenyl acetate-induced responses in *Drosophila*. *J Neurosci* **26**, 8727 (Aug 23, 2006).

27. E. A. Hallem, M. G. Ho, J. R. Carlson, The molecular basis of odor coding in the *Drosophila* antenna. *Cell* **117**, 965 (Jun 25, 2004).

28. E. A. Hallem, J. R. Carlson, Coding of odors by a receptor repertoire. *Cell* **125**, 143 (Apr 7, 2006).

29. E. Fishilevich, L. B. Vosshall, Genetic and functional subdivision of the *Drosophila* antennal lobe. *Curr Biol* **15**, 1548 (Sep 6, 2005).

30. D. A. Wagh *et al.*, Bruchpilot, a protein with homology to ELKS/CAST, is required for structural integrity and function of synaptic active zones in *Drosophila*. *Neuron* **49**, 833 (Mar 16, 2006).

31. M. C. Stensmyr, T. Dekker, B. S. Hansson, Evolution of the olfactory code in the *Drosophila melanogaster* subgroup. *Proc Biol Sci* **270**, 2333 (Nov 22, 2003).

32. M. de Bruyne, R. Smart, E. Zammit, C. G. Warr, Functional and molecular evolution of olfactory neurons and receptors for aliphatic esters across the

Drosophila genus. *J. Comp. Physiol. A Neuroethol. Sens. Neural Behav. Physiol.* **196**, 97 (Feb, 2010).

33. L. L. Prieto-Godino *et al.*, Evolution of acid-sensing olfactory circuits in drosophilids. *Neuron* **93**, 661 (Feb 08, 2017).
34. S. Pop *et al.*, The role of cell death in sculpting functional and adaptive neural networks in flies. *bioRxiv*, 10.1101/626465 (2019).
35. M. Saina, R. Benton, Visualizing olfactory receptor expression and localization in *Drosophila*. *Methods in Molecular Biology* **1003**, 211 (2013).
36. J. A. Sanchez-Alcaniz, G. Zappia, F. Marion-Poll, R. Benton, A mechanosensory receptor required for food texture detection in *Drosophila*. *Nat Commun* **8**, 14192 (Jan 27, 2017).
37. J. Schindelin *et al.*, Fiji: an open-source platform for biological-image analysis. *Nat Methods* **9**, 676 (Jun 28, 2012).
38. J. Ollion, J. Cochennec, F. Loll, C. Escude, T. Boudier, TANGO: a generic tool for high-throughput 3D image analysis for studying nuclear organization. *Bioinformatics* **29**, 1840 (Jul 15, 2013).
39. R. Benton, A. Dahanukar, Electrophysiological recording from *Drosophila* olfactory sensilla. *Cold Spring Harb Protoc* **2011**, 824 (2011).
40. S. B. Olsson, B. S. Hansson, Electroantennogram and single sensillum recording in insect antennae. *Methods Mol Biol* **1068**, 157 (2013).
41. M. Martin, Cutadapt removes adapter sequences from high-throughput sequencing reads. *EMBnet.journal* **17**, (2011).

42. M. P. Davis, S. van Dongen, C. Abreu-Goodger, N. Bartonicek, A. J. Enright, Kraken: a set of tools for quality control and analysis of high-throughput sequence data. *Methods* **63**, 41 (Sep 1, 2013).

43. A. Dobin *et al.*, STAR: ultrafast universal RNA-seq aligner. *Bioinformatics* **29**, 15 (Jan 1, 2013).

44. S. Anders, P. T. Pyl, W. Huber, HTSeq--a Python framework to work with high-throughput sequencing data. *Bioinformatics* **31**, 166 (Jan 15, 2015).

45. L. Wang, S. Wang, W. Li, RSeQC: quality control of RNA-seq experiments. *Bioinformatics* **28**, 2184 (Aug 15, 2012).

46. M. D. Robinson, D. J. McCarthy, G. K. Smyth, edgeR: a Bioconductor package for differential expression analysis of digital gene expression data. *Bioinformatics* **26**, 139 (Jan 1, 2010).

47. M. E. Ritchie *et al.*, limma powers differential expression analyses for RNA-sequencing and microarray studies. *Nucleic Acids Res.* **43**, e47 (Apr 20, 2015).

48. B. Langmead, S. L. Salzberg, Fast gapped-read alignment with Bowtie 2. *Nat Methods* **9**, 357 (Mar 4, 2012).

49. Y. Benjamini, Y. Hochberg, Controlling the False Discovery Rate: A Practical and Powerful Approach to Multiple Testing. *Journal of the Royal Statistical Society. Series B (Methodological)* **57**, 289 (1995).

50. K. Katoh, D. M. Standley, MAFFT multiple sequence alignment software version 7: improvements in performance and usability. *Mol. Biol. Evol.* **30**, 772 (Apr, 2013).

51. H. K. Dweck *et al.*, Pheromones mediating copulation and attraction in *Drosophila*. *Proceedings of the National Academy of Sciences of the United States of America* **112**, E2829 (May 26, 2015).

52. L. B. Vosshall, A. M. Wong, R. Axel, An olfactory sensory map in the fly brain. *Cell* **102**, 147 (Jul 21, 2000).

53. R. Benton, K. S. Vannice, L. B. Vosshall, An essential role for a CD36-related receptor in pheromone detection in *Drosophila*. *Nature* **450**, 289 (Nov 8, 2007).

Acknowledgements

We are grateful to I. Alali and M. Erdogmus for technical assistance, Darren Williams and Sînziana Pop for sharing flies and discussions, Raquel Alverez Ocana for sharing information on neurons numbers, Mattias Alenius, the Bloomington *Drosophila* Stock Center (NIH P40OD018537), and the Developmental Studies Hybridoma Bank (NICHD of the NIH, University of Iowa) for reagents. We thank Roman Arguello and members of the Benton laboratory for comments on the manuscript. **Funding**: L.L.P.-G. was supported by a FEBS Long-Term Fellowship. M.A.K., B.S.H., and M.K. are supported by the Max Planck Society. Research in R.B.'s laboratory is supported by the University of Lausanne, an ERC Consolidator Grant (615094) and the Swiss National Science Foundation. **Author contributions**:

L.L.P.-G. and R.B. conceived the project. All authors contributed to experimental design, analysis and interpretation of results. Experimental contributions were as follows: L.L.P.-G. (Fig. 2; Fig. 3e; Fig. 4a; ED Fig. 1); A.F.S. (Fig. 1d-f; Fig. 3e,f; Fig. 4b-e; ED Fig. 1, ED Fig. 2c,e), M.A.K. (Fig. 5 and ED Fig. 3), S.C. (Fig. 3a,c,d and ED Fig. 2a-d). K.B. and S.P. performed RNA-seq data analysis. R.B., L.L.P.-G. and A.F.S. wrote the paper with input from all other authors. **Competing interests**: the authors declare no competing interests. **Data and materials availability:** all relevant data and materials supporting the findings of this study are available from the corresponding author on request. RNA-seq data are available in GEO (Accession GSE128725).

List of Supplementary Materials

Materials and Methods

Figures S1-S3

Tables S1-S4

Data S1-S4

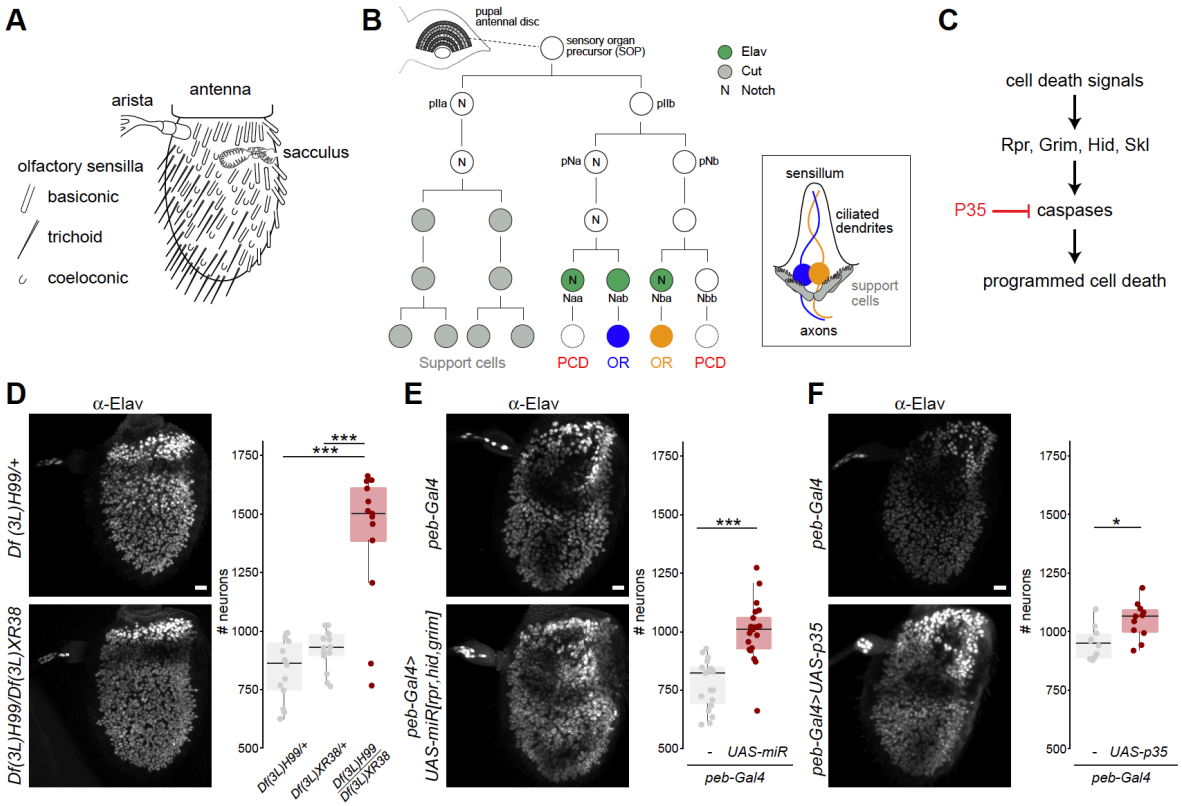

Fig. 1. Inhibition of developmental programmed cell death results in increased neuron numbers in the antenna.

(A) Schematic of the *Drosophila* third antennal segment showing the different sensory structures.

(B) Schematic of the lineage of an antennal disc sensory organ precursor (SOP) giving rise to a sensillum containing two neurons (illustrated on the right). The expression of a subset of molecular markers is shown; Elav is expressed in only three of four neural precursors; one of these (Naa) as well as the Elav-negative cell (Nbb) are eliminated by PCD. The lineage is based upon data from (*13, 14, 20*).

(C) Simplified schematic of the PCD pathway in *Drosophila*, highlighting the elements relevant for this study. Several intermediate steps between the pro-apoptotic proteins (Rpr, Grim, Hid and Skl) and the executioner caspases are not

shown.

(D) Elav expression in whole-mount antennae from control (*Df(3L)H99/+*; the wild-type chromosome here and in other genotypes was derived from a w^{1118} parent) and PCD-deficient (*Df(3L)H99/Df(3L)XR38*) animals. Scale bar = 10 μm. Right: quantifications of antennal neuron numbers of the indicated genotypes, including an additional control genotype (*Df(3L)XR38)/+*). *** indicates p = 0.0007216 for the comparison to *Df(3L)H99/+* and p = 0.0013224 for the comparison to *Df(3L)XR38/+* (Wilcoxon-sum rank test, corrected for multiple comparisons using a Bonferroni correction). In this and subsequent panels, individual data points are shown, overlaid with boxes indicating the median and first and third quartile of the data; whiskers showing the limits of the distribution.

(E) Elav expression in whole-mount antennae from control (*peb-Gal4/+*) and PCD-blocked (*peb-Gal4/+;UAS-miR(grim,rpr,hid)*) animals. Scale bar = 10 μm. Right: quantifications of neuron numbers of these genotypes. *** indicates p = 0.0024×10^{-4} (t-test).

(F) Elav expression in whole-mount antennae from control (*peb-Gal4/+*) and PCD-blocked (*peb-Gal4/+;UAS-p35/+*) animals. Scale bar = 10 μm. Right: quantifications of neuron numbers of these genotypes. * indicates p = 0.024 (t-test).

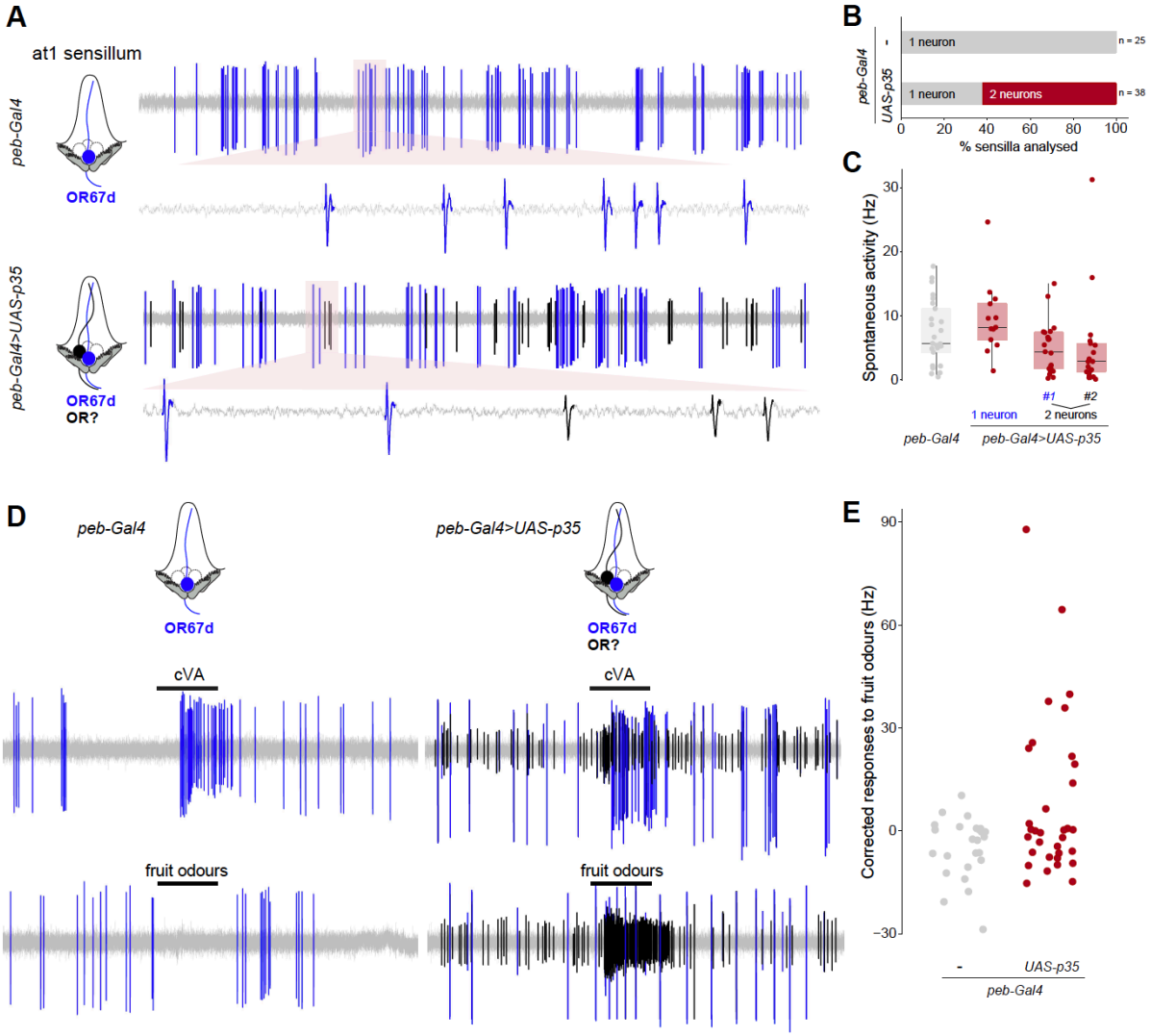

Fig. 2. Undead olfactory sensory neurons are functional.

(A) Representative extracellular electrophysiology traces of spontaneous activity from neurons in an at1 sensillum of control (*peb-Gal4/+*) and PCD-blocked (*peb-Gal4/+;UAS-p35/+*) animals. Automatically-detected spikes (see Materials and Methods) from the neuron expressing OR67d are shown in blue, and those of the additional, undead neuron(s) in black, as schematized in the cartoon on the left (cells fated to die are shown with dashed outlines).

(B) Quantifications of the proportion of sensilla containing either one neuron (grey) or

two (or more) neurons (red) in control (*peb-Gal4/+*) and PCD-blocked (*peb-Gal4/+;UAS-p35/+*) animals.

(C) Quantifications of the spontaneous activity of the indicated neurons for the control and PCD-blocked genotypes.

(D) Representative electrophysiology traces from at1 sensillum recordings in control (*peb-Gal4/+*) and PCD-blocked (*peb-Gal4/+;UAS-p35/+*) animals upon stimulation with a 0.5 s pulse (black horizontal bar) of the pheromone *11-cis*-vaccenyl acetate (cVA) (10^{-2} dilution (v/v) in paraffin oil) or a mix of fruit odors (butyl acetate, ethyl butyrate, *2*-heptanone, hexanol, isoamyl acetate, pentyl acetate; each odor at 10^{-2} dilution (v/v) in paraffin oil). Automatically-detected spikes from the neuron expressing OR67d are shown in blue, and those of the undead neuron(s) in black.

(E) Quantifications of odor-evoked responses to fruit odors (see Materials and Methods) in control (*peb-Gal4/+*) and PCD-blocked (*peb-Gal4/+;UAS-p35/+*) animals.

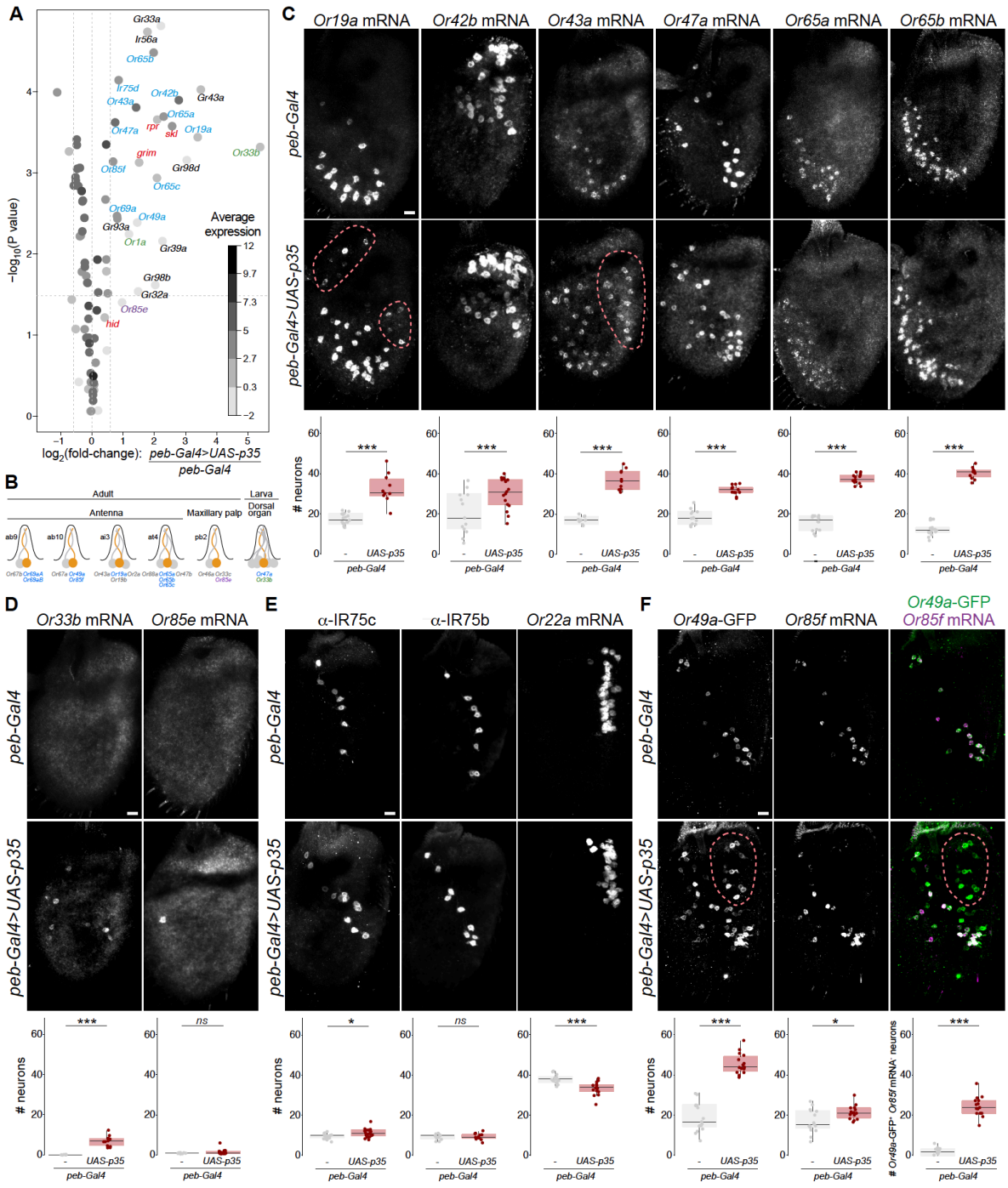

Fig. 3. Undead neurons express a subset of olfactory receptor genes.

(A) Gene expression differences between control and PCD-blocked antennae. The volcano plot shows the differential expression (on the x-axis) of *D. melanogaster Or*, *Ir* and *Gr* gene transcripts (each gene represented by a dot), as well as the four pro-

apoptotic genes (*grim*, *rpr*, *hid* and *skl*; red labels), plotted against the statistical significance (on the y-axis). The mean expression level of individual genes across all samples is shown by the shading of the dot, as indicated by the grey scale on the right (units: $\log_2$(counts per million)). Only chemosensory genes showing a >1.5-fold increase in PCD-blocked antennae are labelled: blue labels indicate genes whose expression in the antenna has previously been demonstrated by RNA *in situ* hybridisation; magenta and green labels indicate receptors normally only expressed in the adult maxillary palps and larval dorsal organ, respectively; black labels indicate receptors that are expressed in gustatory organs. The horizontal dashed line indicates a false discovery rate threshold of 5%. Data for all *Or*, *Ir* and *Gr* genes are provided in Data S2.

(B) Schematic summarising the normal olfactory organ/sensillum expression pattern of the subset of up-regulated *Or* genes that display co-expression in wild-type neurons (color-coded as in **(A)**; genes showing no changes in transcript levels are labelled in grey).

(C) Representative images of RNA FISH for the indicated *Or* genes in whole mount antennae of control (*peb-Gal4/+*) and PCD-blocked (*peb-Gal4/+;UAS-p35/+*) animals. Scale bar = 10 μm. Quantifications of neuron numbers are shown at the bottom. *** indicates *Or19a* p = 6.526 x 10^{-05} (t-test), *Or42b* p = 0.008486 (t-test), *Or65a* p = 4.701 x 10^{-06} (Wilcoxon-sum rank test), *Or43a* p = 5.888x10^{-07} (t-test) (see also Fig. S2A). The pink dashed line encircles those cells in the PCD-blocked antenna that express the corresponding *Or*s outside their usual spatial domain (see also Fig. S2B).

(D) Representative images of RNA FISH for the indicated *Or* genes in whole mount antennae of control (*peb-Gal4/+*) and PCD-blocked (*peb-Gal4/+;UAS-p35/+*) animals. Scale bar = 10 μm. Quantifications of neuron numbers are shown at the bottom.. *** indicates *Or33a* p = 1.812×10^{-07} (t-test), *Or85e* p = 0.053 (Wilcoxon-sum rank test).

(E) Representative images of immunohistochemistry or RNA FISH for the indicated olfactory receptors in whole mount antennae of control (*peb-Gal4/+*) and PCD-blocked (*peb-Gal4/+;UAS-p35/+*) animals. Scale bar = 10 μm. Quantifications of neuron numbers are shown at the bottom. *, ns, and *** indicate, respectively, IR75c p = 0.01 (t-test), IR75b p = 0.9246 (t-test), *Or22a* p = 0.0002472 (t-test).

(F) Representative images of anti-GFP and RNA FISH for *Or85f* in whole mount antennae of control (*peb-Gal4/+;Or49a-GFP/+*) and PCD-blocked (*peb-Gal4/+;Or49a-GFP/UAS-p35*) animals. Scale bar = 10 μm. Quantifications of neuron numbers are shown at the bottom. *** indicates *Or49a-GFP* p = 1.444×10^{-12} (t-test), *Or85f* p = 0.01375 (t-test), merged panel *Or49a-GFP*$^{+}$/Or85f mRNA^{-} population p = 5.48×10^{-12} (t-test). The pink dashed line encircles those cells in the PCD-blocked antenna that express *Or49a*-GFP outside its usual spatial domain. We used an *Or49a-GFP* reporter, due to our inability to reliably detect *Or49a* transcripts *in situ*; the higher number of *Or49a-CD8:GFP*-positive *Or85f* RNA-positive cells is not an artefact of the analysis method, as an *Or85f*-CD8:GFP reporter revealed a similarly limited increase in neuron number (Fig. S2E).

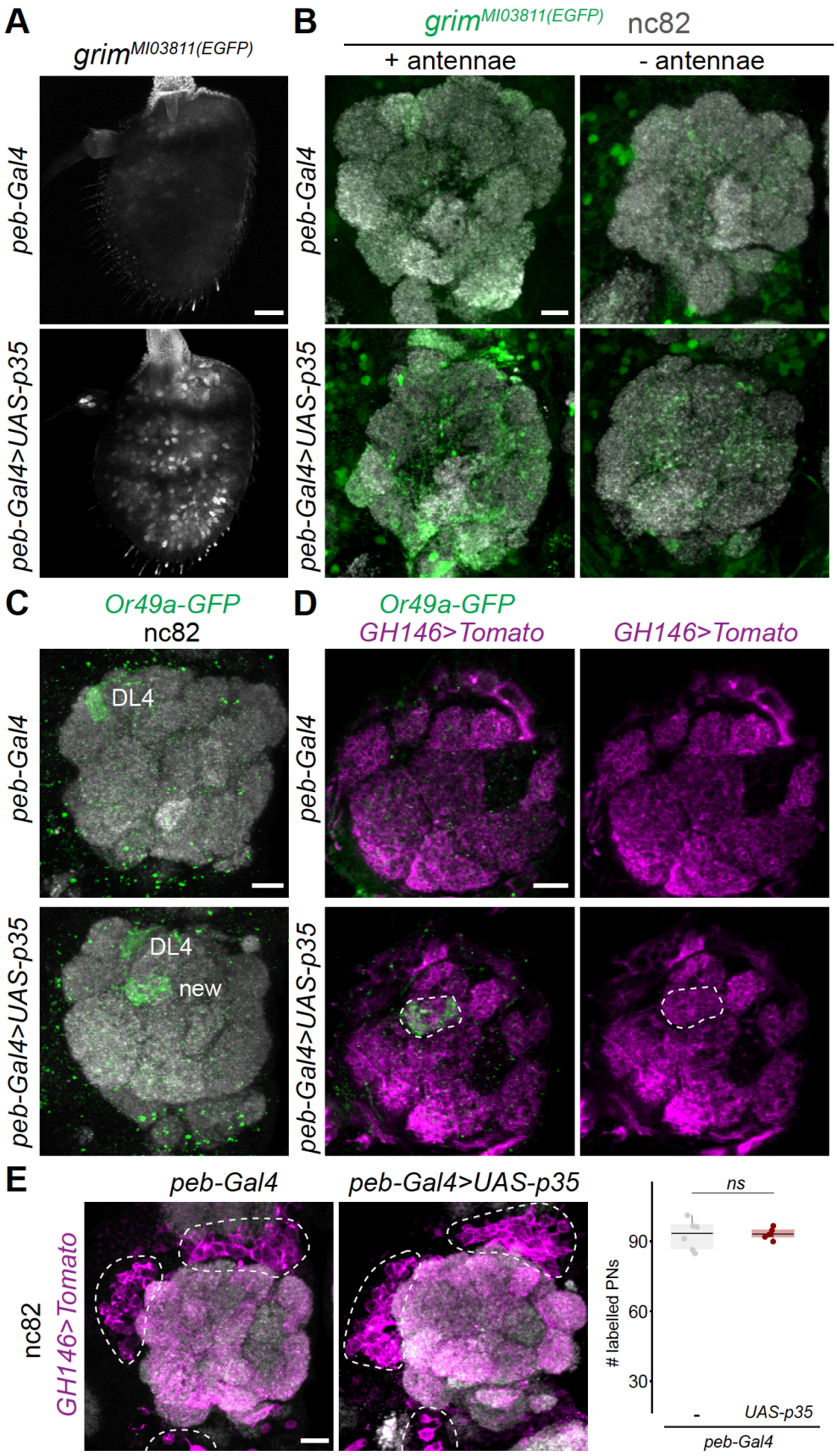

Fig. 4. Undead olfactory sensory neurons form novel wiring properties in the brain.

(A) Representative images of anti-GFP immunofluorescence in whole mount antennae of control (*peb-Gal4/+;+;grim*$^{MI03811(EGFP)}$*/+*) and PCD-blocked (*peb-Gal4/+; UAS-p35/+;grim*$^{MI03811(EGFP)}$*/+*) animals. Blind scoring by two independent observers of antennae as belonging to control or PCD-blocked group was 100% accurate (see Materials and Methods). Scale bar = 10 μm.

(B) Representative images of combined anti-GFP and nc82 immunofluorescence in whole mount brains of control (*peb-Gal4/+;;grim*$^{MI03811(EGFP)}$*/+*) and PCD-blocked (*peb-Gal4/+;UAS-p35/+;grim*$^{MI03811(EGFP)}$*/+*) animals with intact (left) or excised antennae (right). Blind categorisation of brains (n = 9-12 brains per genotype) as belonging to the control or PCD-blocked set was 95% accurate (2 independent observers). Scale bar = 10 μm.

(C) Representative images of combined anti-GFP and nc82 immunofluorescence in whole mount brains of control (*peb-Gal4/+;Or49a-GFP/Or49a-GFP;GH146-QF,QUAS-Tomato/+*) and PCD-blocked (*peb-Gal4/+;Or49a-GFP/Or49a-GFP,UAS-p35;GH146-QF,QUAS-Tomato/+*) animals. Blind categorisation of brains (n = 9 and 7 brains, respectively, per genotype) as belonging to the control or PCD-blocked group was 100% accurate (1 observer). Scale bar = 10 μm.

(D) Representative images of combined anti-GFP, anti-RFP and nc82 immunofluorescence in whole mount brains of control (*peb-Gal4/+;Or49a-GFP/Or49a-GFP;GH146-QF,QUAS-Tomato/+*) and PCD-blocked (*peb-Gal4/+;Or49a-GFP/Or49a-GFP, UAS-p35;GH146-QF,QUAS-Tomato/+*) animals.

Scale bar = 10 μm.

(E) Representative images of PN soma (bounded by the dashed lines) labelled by GH146>Tomato in whole mount brains of control (*peb-Gal4/+;Or49a-GFP/ Or49a-GFP;GH146-QF,QUAS-Tomato/+*) and PCD-blocked (*peb-Gal4/+;Or49a-GFP/Or49a-GFP,UAS-p35;GH146-QF,QUAS-Tomato/+*) animals. Scale bar = 10 μm. Quantifications of neuron numbers are shown to the right. *ns* indicates p = 0.819 (t-test).

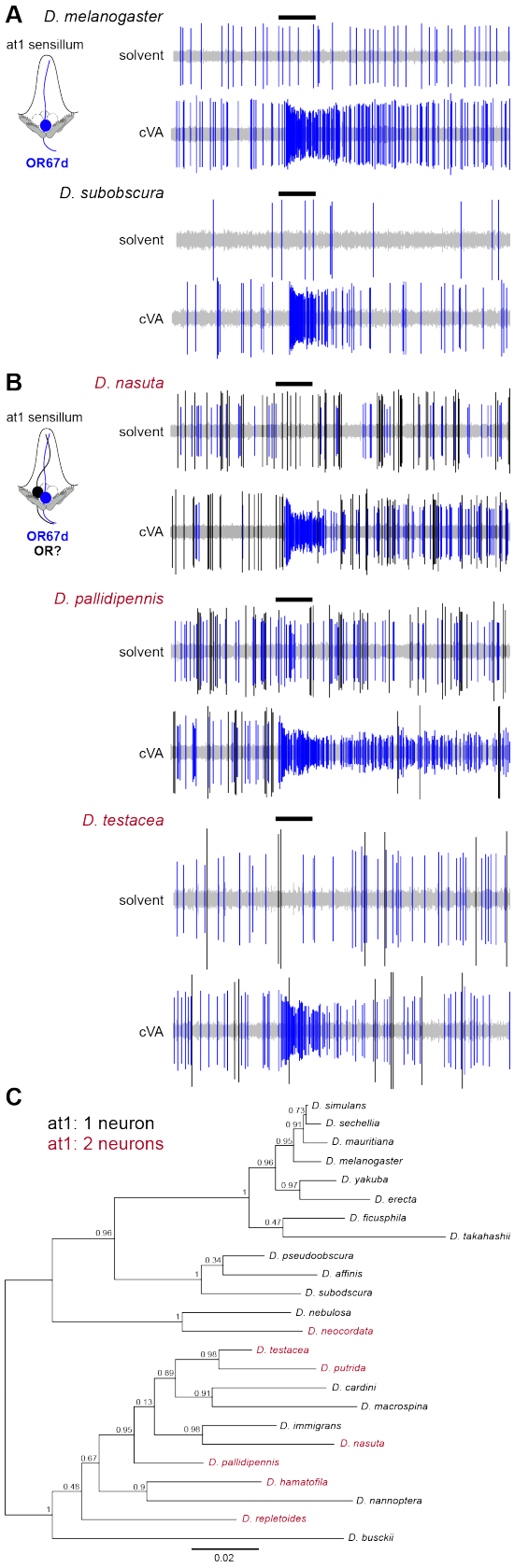

Fig. 5. Examples of naturally occurring extra neurons in at1 sensilla.

(A) Representative traces of extracellular recordings of neuronal responses to a 0.5 s pulse (black horizontal bar) of solvent (dichloromethane) or cVA in *D. melanogaster* and *D. subobscura* (n = 5). A single cVA-responsive neuron (known or assumed to express OR67d orthologs) is detected (blue spikes), as schematized in the cartoon on the left.

(B) Representative traces of extracellular recordings of neuronal responses to a 0.5 s pulse (black horizontal bar) of solvent (dichloromethane) or cVA in *D. nasuta, D. pallidipennis* and *D. testacea* (n = 3-5). Two spike amplitudes are detected: a cVA-responsive neuron (assumed to express OR67d orthologs) (blue spikes) and second neuron with a larger spike amplitude, which does not respond to cVA (black spikes), as schematized in the cartoon on the left.

(C) Phylogeny of 24 drosophilid species, representing the majority of the *Drosophila* genus subgroups, based on the protein sequences of housekeeping loci (see Materials and Methods). Species names are colored to reflect the presence of one or two neurons in at1 sensilla. Numbers next to the tree nodes indicate the support values. The scale bar for branch length represents the number of substitutions per site.

Functional integration of "undead" neurons in the olfactory system

Lucia L. Prieto-Godino, Ana F. Silbering, Mohammed A. Khallaf, Steeve Cruchet, Karolina Bojkowska, Sylvain Pradervand, Bill S. Hansson, Markus Knaden and Richard Benton

Supplementary Information

Materials and Methods

Drosophila culture

Flies were maintained at 25ºC in 12 h light:12 h dark conditions, except where noted. *D. melanogaster* strains were cultured on a standard cornmeal diet; other drosophilid species were grown on food sources as indicated in Table S4 (for recipes: http://blogs.cornell.edu/drosophila/recipes). Published mutant and transgenic *D. melanogaster* are described in Table S4. *Df(3L)H99/Df(3L)XR38* (and their controls) were cultured at 22ºC to increase the number obtained of adult offspring of the desired genotype. For most histological experiments, only female flies were analysed, to avoid confounding variation due to known sexual dimorphisms (*17*). Mixed genders were used for *Df(3L)H99/Df(3L)XR38* flies in Fig. 1D due to the limitation in the recovery of this genotype, as well as for anti-IR75b and anti-IR75c immunofluorescence in Fig. 3E (there is no sexual dimorphism in the numbers of these OSNs). For histological experiments, flies were 1-12 days old. Animals subjected to antennal deafferentation (and control intact flies) were left for 10 days post-surgery to permit degeneration of OSN axons. For the experiments in Fig. 5 and Fig. S3, all experiments were carried out with 8-15 day old, mated female flies.

Histology and image analysis

Whole mount antennal immunofluorescence and RNA fluorescent *in situ* hybridisation were performed essentially as described (*35*). Whole mount brain immunofluorescence was performed essentially as described (*36*). Primary and secondary antibodies are listed in Table S5. Sources and/or construction details of templates for RNA probes are provided in Table S6. Imaging was performed on a Zeiss confocal microscope LSM710 or LSM880 using a 40x oil immersion objective.

For automated counting of Elav-positive cell bodies, confocal stacks were imported into Fiji (*37*) and passed through a median 3D filter of radius 1 in all dimensions. Images were subsequently thresholded using the 3D iterative thresholding plug-in (*38*), and cells automatically counted using the 3D object counter.

Analyses of OSN numbers expressing specific olfactory receptor genes, and morphological differences of the antennal lobes of control and PCD-blocked animals were performed by experimenters blind to the genotype, using RandomNames.bat (https://github.com/DavidOVM/File-Name-Randomizer/blob/master/RandomNames.bat) to encode image names.

Electrophysiology

Single-sensillum recordings were performed and analysed essentially as described (*39, 40*). at1 sensilla were identified based upon their morphology and characteristic distal distribution on the antenna; they could also be clearly distinguished from the only other trichoid sensillum class, at4, which houses three OSNs (Fig. S3 and data not shown). Chemical stimuli and solvents are described in Table S7. For the experiments in Fig. 2, neuron activity was recorded for 10 s, starting 3 s before a stimulation period of 0.5 s. For the experiments in Fig. 5 and Fig. S3, neuron activity was recorded for 6 s, starting 2 s before a stimulation period of 0.5 s. Traces were analysed by sorting spike amplitudes in AutoSpike; representative traces presented in the figures were further processed in Adobe Illustrator CS (Adobe systems, San Jose, CA). Spontaneous neuron activity was quantified by counting spontaneous spikes in a 10 s recording window. Stimulus-evoked activity was quantified by counting spikes in a 0.5 s window during odor stimulation, and then subtracting this count from a 0.5 s recording window just prior to stimulation. For the solvent-corrected quantifications in Fig. 2D-E, the responses to solvent (paraffin oil) were subtracted from the responses to the odor. In Fig. 2B, sensilla were classified as having two neurons if two different spike amplitudes were automatically detected and/or corrected responses to the fruit odor mix were above 20 Hz.

RNA-sequencing and analysis

Antennal RNA was extracted from three biological replicates of control (*peb-Gal4/+;Or49a-GFP/+*) and PCD-blocked (*peb-Gal4/+;Or49a-GFP/UAS-p35*) animals. (The increased numbers of neurons labelled by *Or49a-GFP* was noted in preliminary studies and we therefore incorporated this transgene into the genotypes used in these experiments as an internal control; see below). For each pair of biological replicates, ~200 animals were grown under identical conditions and RNA was extracted in parallel using 2-5 day old flies, as described (*20*). RNA quality was assessed on a Fragment Analyzer (Advanced Analytical Technologies, Inc.); all RNAs had an RQN of 9.8-10. From 100 ng total RNA, mRNA was isolated with the NEBNext Poly(A) mRNA Magnetic Isolation Module. RNA-seq libraries were prepared from the mRNA using the NEBNext Ultra II Directional RNA Library Prep Kit for Illumina (New England Biolabs). Cluster generation was performed with the resulting libraries using the Illumina TruSeq PE Cluster Kit v4 reagents and sequenced on the Illumina HiSeq 2500 using TruSeq SBS Kit v4 reagents (Illumina). Sequencing data were demultiplexed using the bcl2fastq Conversion Software (version 2.20, Illumina).

Purity-filtered reads were adapters- and quality-trimmed with Cutadapt (version 1.8 (*41*)). Reads matching to ribosomal RNA sequences were removed with fastq_screen (version 0.11.1). Remaining reads were further filtered for low complexity with reaper (version 15-065) (*42*). Reads were aligned to the *Drosophila melanogaster* BDGP6.92 genome using STAR (version 2.5.3a (*43*)). The number of read counts per gene locus was summarized with htseq-count (v. 0.9.1) (*44*) using *Drosophila melanogaster*.BDGP6.92 gene annotation. The quality of the RNA-seq data alignment

was assessed using RSeQC (v. 2.3.7) (*45*).

Statistical analysis was performed for genes in R (version 3.5.3). Genes with low counts were filtered out according to the rule of 1 count per million in at least 1 sample. Library sizes were scaled using TMM normalisation (EdgeR package version 3.24.3) (*46*) and log-transformed with limma cpm function (Limma package version 3.38.3) (*47*).

Differential expression was computed with limma for paired samples by fitting the 6 samples into a linear model and performing the comparison PCD-blocked antennae versus controls. Comparison of read number for *GFP* (encoded by the *Or49a-GFP* transgene) was performed by mapping reads to the *GFP* sequence with Bowtie2 (*48*): control antennal RNA: 139±9.5 reads/sample (mean ± standard deviation); PCD-blocked antennal RNA: 227±8.7 reads/sample.

Moderated t-test was used for the comparison on a subset of 83 expressed *D. melanogaster* genes including: *Or, Ir* and *Gr* genes as well as the four pro-apoptotic genes (*grim*, *rpr*, *hid* and *skl*). For multiple testing correction, the *p*-values were adjusted by the Benjamini-Hochberg method, which controls the false discovery rate (*49*). The volcano plot was generated in R by plotting the $\log_2$(fold change PCD-blocked vs control) against the -log(p value). Data points were shaded according to mean expression value across all samples.

Phylogenetic analysis

Phylogenetic analysis of drosophilid species was conducted using 6 housekeeping proteins, encompassing two nuclear loci (*Adh* and Xdh) and four mitochondrial loci (*COI*, *COII*, *COIII* and *ND2*). Available amino acid sequences from Uniprot (https://www.uniprot.org, accession numbers are listed in Table S8) of each species were concatenated in Geneious (v11.0.5). A multiple sequence alignment of 2939 positions was generated using the MAFFT (v7.309) tool with E-INS-I parameters and scoring matrix 200 PAM / K=2 (*50*). The final tree was reconstructed using a maximum likelihood approach with the GTR+G+I model of nucleotide substitution and 1000 rate categories of sites in FastTree (v2.1.5). The tree was visualized and processed in Geneious (v11.0.5).

Statistics and reproducibility

Statistical analyses and plotting were made in RStudio (v1.1.463 R Foundation for Statistical Computing, Vienna, Austria, 2005; R-project-org), except for the RNA-seq analyses (described above). For statistical analyses, normality was first assessed on datasets using a Shapiro test. If both datasets were normally distributed, a two-sided t-test was performed; otherwise, a Wilcoxon-rank sum test was performed.

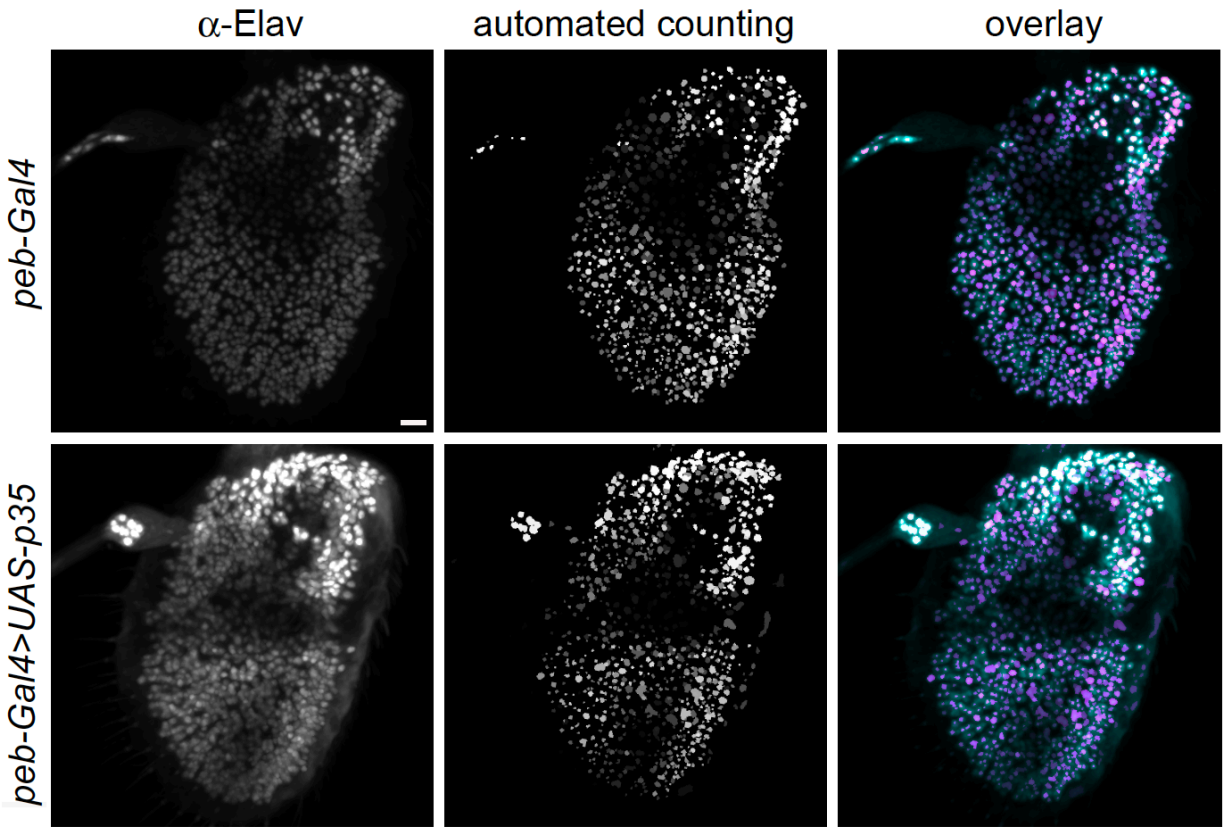

Fig. S1. Automated quantification of Elav-positive olfactory sensory neurons. Representative example of Elav expression in whole-mount antennae from control (*peb-Gal4/+*) and PCD-blocked (*peb-Gal4/+;UAS-p35/+*) animals. Middle: output of auto8mated image segmentation of the same antennae used for quantification of OSN number (see Methods). Right: overlay of both images. Scale bar = 10 μm.

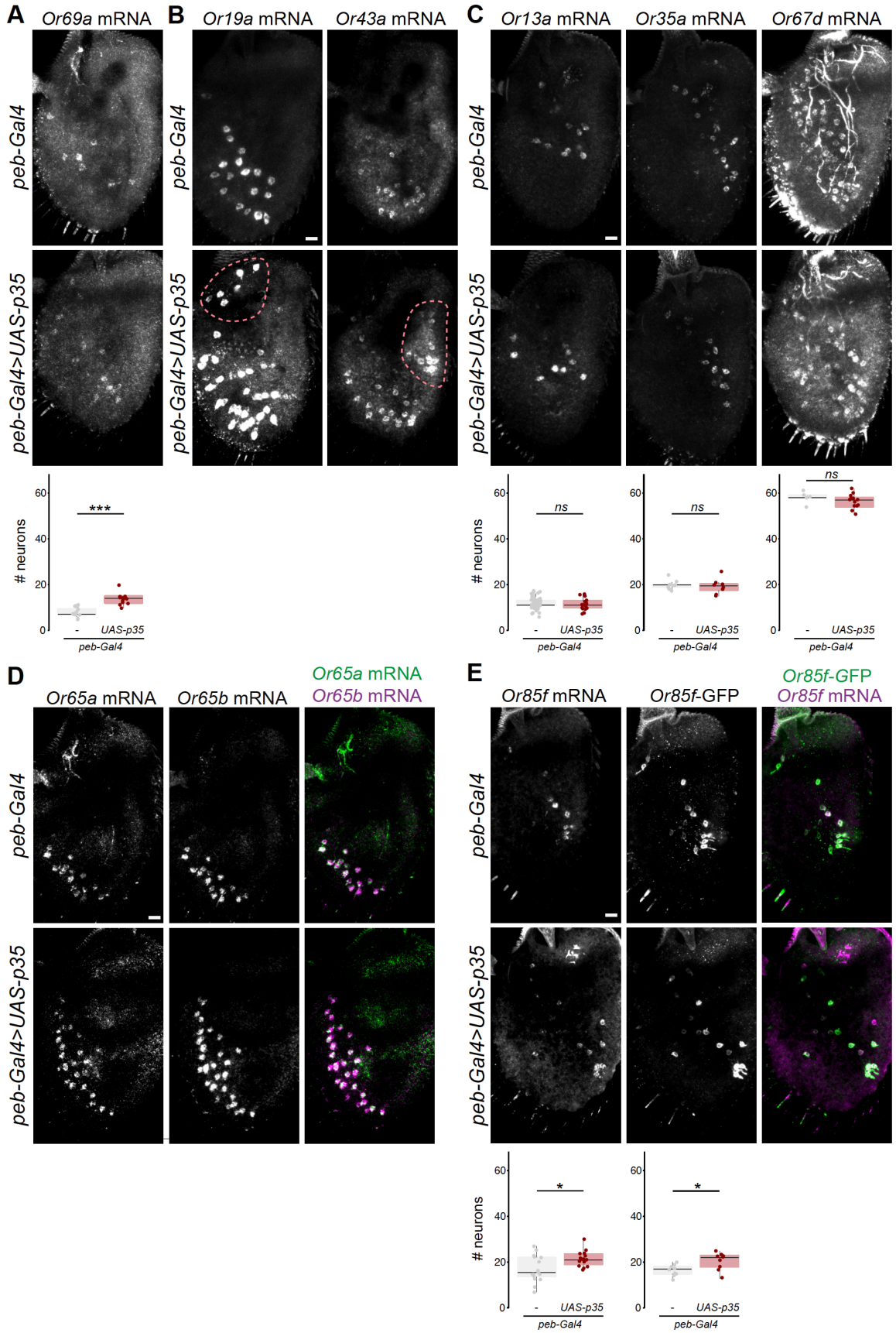

Fig. S2. Characterisation of *Or* expression in PCD-blocked antennae.
(A) Representative images of RNA FISH for *Or69a* in whole mount antennae of control (*peb-Gal4/+*) and PCD-blocked (*peb-Gal4/+;UAS-p35/+*) animals. Scale bar = 10 μm. Quantifications of neuron numbers are shown at the bottom. *** indicates p = 1.811 x 10^{-05} (Wilcoxon-sum rank test).
(B) Additional representative images of RNA FISH for *Or19a* and *Or43a* in whole mount antennae of control (*peb-Gal4/+*) and PCD-blocked (*peb-Gal4/+;UAS-p35/+*) animals. Scale bar = 10 μm. The pink dashed line encircles those cells in the PCD-blocked antenna that express *Or*s outside their usual spatial domain.
(C) Representative images of RNA FISH for the indicated *Or* genes in whole mount antennae of control (*peb-Gal4/+*) and PCD-blocked (*peb-Gal4/+;UAS-p35/+*) animals. Quantifications of neuron numbers are shown at the bottom. Scale bar = 10 μm. *ns* indicates *Or13a* p = 0.4759, *Or35a* p = 0.7132 (t-test), *Or67d* p = 0.05341 (Wilcoxon-sum rank test).
(D) Representative images of combined RNA FISH for *Or65a* (green) and *Or65b* (magenta) in whole mount antennae of control (*peb-Gal4/+*) and PCD-blocked (*peb-Gal4/+;UAS-p35/+*) animals, showing co-expression of these receptors in both endogenous and undead neurons. Scale bar = 10 μm.
(E) Representative images of RNA FISH for *Or85f* and anti-GFP in whole mount antennae of control (*peb-Gal4/+;Or85f-GFP/+*) and PCD-blocked (*peb-Gal4/+;Or85f-GFP/UAS-p35*) animals. Scale bar = 10 μm. Quantifications of neuron numbers are shown at the bottom. * indicates *Or85f* mRNA p = 0.01375 (t-test), GFP p = 0.0153 (t-test).

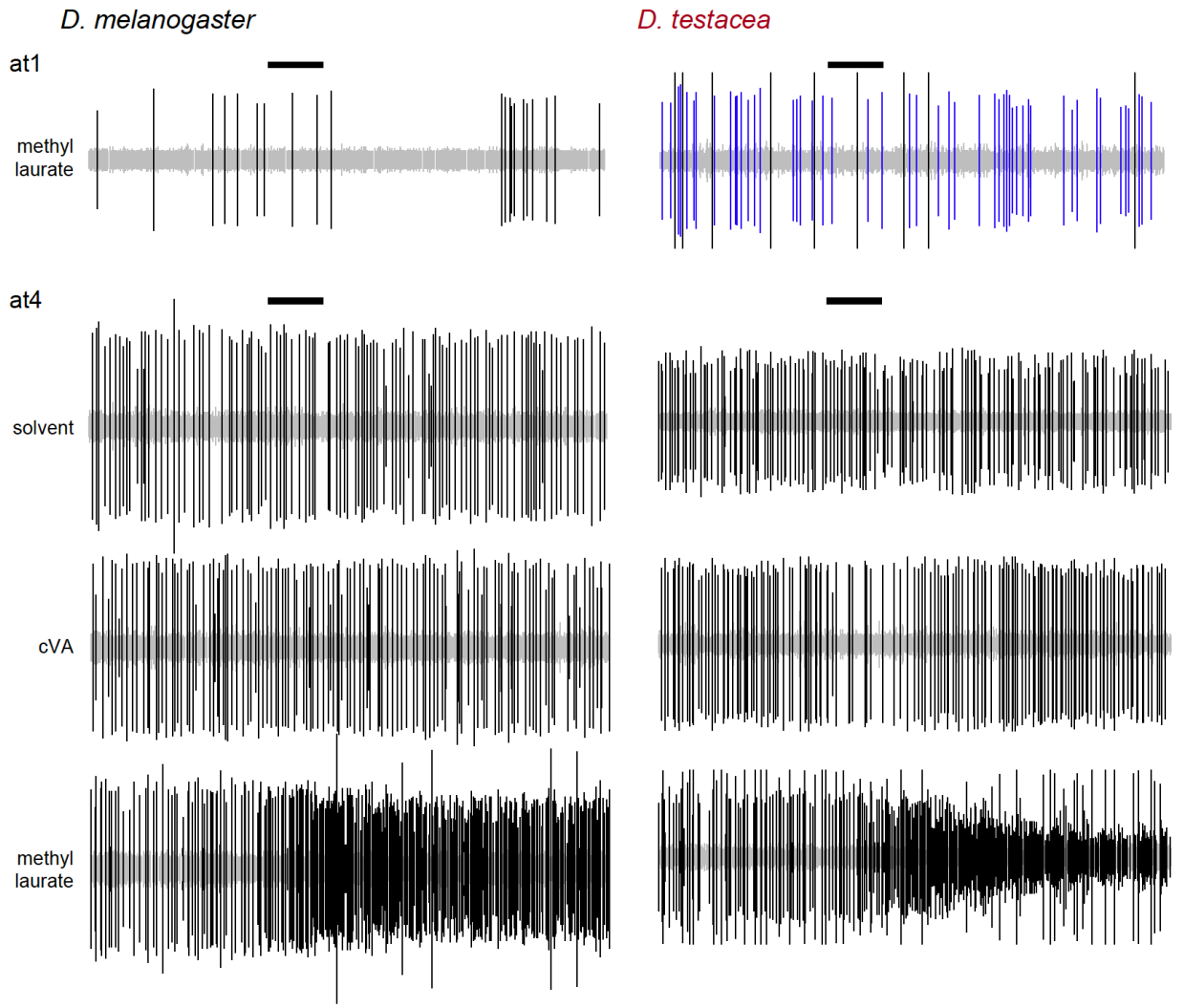

Fig. S3. Electrophysiological distinction of at1 and at4 sensilla.
Representative traces of extracellular recordings of neuronal responses to a 0.5 s pulse (black horizontal bar) of methyl laurate (diluted 1:10 v/v), cVA (1:10) or solvent (dichloromethane) in at1 or at4 sensilla of *D. melanogaster* and *D. testacea* (n = 5). Methyl laurate permits functional distinction of these sensillum classes, as it does not activate the Or67d neuron in *D. melanogaster*, or either neuron in the 2-neuron at1 sensilla of *D. testacea*; by contrast, this pheromone robustly activates at4 sensilla neurons (corresponding to the Or47b and Or88a neuron classes in *D. melanogaster* (*51*)).

Table S1. Drosophilid stocks.

Genotype	Source	Reference
w^{1118}		
peb-Gal4	L. Luo	(*24*)
UAS-p35	BDSC	BL-5072
UAS-miR(grim,rpr,hid)	D. Williams	(*22*)
Df(3L)H99	BDSC	BL-1576
Df(3L)XR38	BDSC	BL-2099
Mi {MIC}grim^{MI03811}	BDSC	BL-36978
Or49a-CD8:GFP	BDSC	BL-52629
Or85f-CD8:GFP	BDSC	BL-52643
GH146-QF	BDSC	BL-30015
QUAS-Tomato	BDSC	BL-30005
D. affinis (banana)	DSSC	14012-0141.00
D. busckii (banana)	DSSC	13000-0081.00
D. cardini (banana)	DSSC	1518-2181.03
D. erecta (cornmeal)	DSSC	14021-0224.01
D. ficusphila (banana)	DSSC	14025-0441.01
D. hamatofila (banana)	DSSC	15081-1301.05
D. immigrans (cornmeal)	DSSC	15111-1731.10
D. macrospina (banana)	DSSC	15120-1931.00
D. mauritiana (banana)	DSSC	14021-0241.150
D. melanogaster CS (cornmeal)		
D. nannoptera (banana)	DSSC	15090-1692.00
D. nasuta (cornmeal)	DSSC	15112-178.01
D. nebulosa (cornmeal)	DSSC	14030-0761.00
D. neocordata (banana)	DSSC	14041-0831.00
D. pallidipennis (banana)	DSSC	15210-2331.02
D. pseudoobscura (banana)	DSSC	14011-0121.00
D. putrida (banana)	DSSC	15150-2101.00
D. repletoides (banana)	DSSC	15250-2451.01
D. sechellia (cornmeal/noni juice)	DSSC	14021-0248.07
D. simulans (cornmeal)	DSSC	14021-0251.01
D. subobscura (banana)	DSSC	14011-0131.04
D. takahashii (cornmeal/blueberry)	DSSC	14022-0311.00
D. testacea (banana)	DSSC	15150-2101.00
D. yakuba (cornmeal)	DSSC	14021-0261.40

Table S2. Antibodies

Antibody	Dilution	Source/Reference
Mouse anti-Elav	1:10	DSHB
Rabbit anti-RFP	1:250	Abcam ab62341
Chicken anti-GFP	1:1000	Abcam ab13970
Rabbit anti-IR75b	1:100	(*33*)
Guinea pig anti-IR75c	1:100	(*33*)
Mouse anti-Bruchpilot (nc82)	1:10	DSHB
Alexa 488 Goat Anti-Chicken	1:1000	Abcam ab150169
Cy3 Goat Anti-Mouse	1:250	Jackson Immunoresearch 115-165-166
Cy3 Goat Anti-Rabbit	1:250	Jackson Immunoresearch 111-165-144 0
Alex488 Goat Anti-Rabbit	1:100	Invitrogen A11034
Cy5 Goat Anti-Mouse	1:250	Jackson Immunoresearch 115-175-166
Cy3 Goat Anti-Rat	1:100	Jackson Immunoresearch 112-166-003

Table S3. Template construction for RNA FISH probes.

RNA probe	Forward / reverse primers (5'-3')	Source
Or19a		(*15*)
Or22a		(*52*)
Or33b		(*15*)
Or42b		(*20*)
Or43a	CCGGTGACTGCGATGAATCT / CTCGTACCAGGGCACATTGT	*This work*
Or47a		(*52*)
Or49a		(*15*)
Or65a		(*15*)
Or65b		(*15*)
Or67a		(*53*)
Or69a		(*52*)
Or85e		(*52*)
Or85f	ATGGAACCTGTGCAGTACAG / CTACTGAATCATCTGCATGAGCA	*This work*

Table S4. Chemical stimuli.

Chemical	Source	CAS
11-cis-vaccenyl acetate	Pherobank (Fig. 2); AKos Consulting Solutions (Fig. 5, Fig. S3)	6186-98-7
butyl acetate	Sigma-Aldrich	123-86-4
ethyl butyrate	Sigma-Aldrich	105-54-4
2-heptanone	Sigma-Aldrich	110-43-0
hexanol	Sigma-Aldrich	111-27-3
isoamyl acetate	Sigma-Aldrich	123-92-2
pentyl acetate	Sigma-Aldrich	628-63-7
methyl laurate	Sigma-Aldrich	111-82-0
dichloromethane	Sigma-Aldrich	75-09-2
paraffin oil	Sigma-Aldrich	8012-95-1

Data S1 (separate file). Estimated potential pool of undead neurons in the antenna.
The number of potential undead neurons in the antenna was calculated from information on the number of each neuron/sensillum class and the number of neurons that are normally removed by PCD. Estimations of neuron numbers are taken from quantification of *Or-* and *Ir-Gal4* driver expression (*17*), except where direct analysis of receptor gene expression is available (by RNA FISH or immunofluorescence, as indicated in the Notes column). As the numbers of neurons for the classes housed in the same sensillum should be identical – but may vary due to technical reasons – the mean of the individual values was calculated to provide a more accurate estimation of the number of each sensillum type, and thereby the total number of antennal neurons; these are largely concordant with previous estimates (*11*). The "# potential undead neurons/sensillum" values are based on the assumption that only three of four potential OSNs express Elav during development (*13*) (except in ab1 where there are four Elav-positive cells); thus, sensilla that house one, two or three neurons, could potentially give rise to two, one or zero additional undead Elav-positive cells if PCD is blocked.
Provided as an accompanying Excel file.

Data S2 (separate file). Comparison of chemosensory receptor and pro-apoptotic factor transcript abundance in control and PCD-blocked antennae.
Provided as an accompanying Excel file.

Data S3 (separate file). *In situ* expression properties of chemosensory genes up-regulated in PCD-blocked antennae.
The chemosensory genes listed are the subset displaying a >1.5-fold increase in expression in PCD-blocked antennae compared to control antennae from Table S2. *In situ* expression data are derived from previous studies (*13, 15, 16, 20, 29*); sensilla name abbreviations are shown in Table S1 (pb = maxillary palp basiconic).
Provided as an accompanying Excel file.

Data S4 (separate file). Accession numbers of the housekeeping protein sequences used to reconstruct the drosophilid phylogenetic tree.
Provided as an accompanying Excel file.